Force-Length Relationship Modeling of Wrist and Finger Flexor Muscles

Hugo Hauraix, Benjamin Goislard de Monsabert, Alexis Herbaut, Eric Berton, Laurent Vigouroux

Force–Length Relationship Modeling of Wrist and Finger Flexor Muscles

HUGO HAURAIX[1], BENJAMIN GOISLARD DE MONSABERT[1], ALEXIS HERBAUT[2], ERIC BERTON[1], and LAURENT VIGOUROUX[1]

[1]Institute of Movement Sciences, Aix-Marseille University, CNRS, ISM, Marseille, FRANCE; and [2]Department of Movement, Sciences, Decathlon Sports Lab, Villeneuve d'Ascq, FRANCE

ABSTRACT

HAURAIX, H., B. GOISLARD DE MONSABERT, A. HERBAUT, E. BERTON, and L. VIGOUROUX. Force–Length Relationship Modeling of Wrist and Finger Flexor Muscles. *Med. Sci. Sports Exerc.*, Vol. 50, No. 11, pp. 2311–2321, 2018. **Introduction**: Because the hand joints possess a broad range of motion, the muscle length can vary importantly which might result in significant variations of the muscle force-generating capacities. However, facing the complexity of this musculoskeletal system, no study has examined the effect of hand muscle length change on muscle force. This study aimed to characterize the force–length relationship of muscles involved in wrist and metacarpophalangeal flexion. **Methods**: Eleven participants performed two sessions: (i) one for the wrist flexor muscles and (ii) one for the finger flexor muscles. For each session, the participants performed two maximal voluntary contractions and then two progressive isometric ramps from 0% to 100% of their maximal force capacity at five different wrist/metacarpophalangeal angles. Torque, kinematic, and electromyographic data were recorded. An ultrasound scanner was used to measure the myotendinous junction displacement of flexor carpi radialis (FCR) and flexor digitorum superficialis (FDS) during isometric contractions. A three-dimensional relationship between muscle length, force, and activation level was modeled using optimization procedure. **Results**: Globally, the FCR was stronger and shorter compared with FDS. The results showed that the three-dimensional relationships fitted well the experimental data (mean R^2 = 0.92 ± 0.07 and 0.87 ± 0.11 for FCR and FDS, respectively). Using joint angle and EMG data, this approach allows to estimate the muscle force with low estimation errors (<9% of F_{max}). **Conclusions**: This study proposes a new method to investigate the force–length relationship by combining ultrasound measurement, musculoskeletal modeling and optimization procedures. The data and relationships provide a new insight into hand biomechanics and muscle function that could be useful for designing hand tools or surgical operations. **Key Words:** ULTRASOUND, FLEXOR CARPI RADIALIS, FLEXOR DIGITORUM SUPERFICIALIS, TENDON, MUSCULOSKELETAL MODEL, MODELING

Hand grasping capabilities are essential for daily life and are involved in during various activities with a wide range of aims: tasks requiring precise grip, for example, manipulating a pen or a needle, tasks requiring accurate finger movements, for example, playing the piano, or tasks requiring high levels of force, for example, pull-ups, handling a tennis racket, hitting with a hammer. This versatility is the result of the unique hand musculoskeletal system, which is one of the most complex in the human body. With a total of 16 joints in the fingers and wrist, the hand can adapt its grip to the shapes and sizes of many tools or objects. These joints are actuated by 42 muscles originating from both the forearm (i.e., extrinsic muscles) and the hand (i.e., intrinsic muscles) is required. Because of this complexity, estimating the force produced by each hand muscle during a task remains challenging, even for the most common ones such as holding a glass of water. The access to such information is however essential for improving pathology prevention and optimizing the human-tool interface, for example, the design of tools or sports equipment.

Although sensors have been developed to obtain *in vivo* direct measurements of tendon forces in isolated finger muscles (1), such techniques are highly invasive and cannot be used to simultaneously record all the muscles/tendons actuating the hand. Musculoskeletal models represent a noninvasive solution for estimating the loadings withstood by the muscles and other internal structures such as joints and ligaments. Many models have been developed to study the lower and upper limbs (2). Based on dynamometric, kinematic and electromyographic (EMG) data, these models rely on optimization processes to solve the muscle redundancy problem, while respecting mechanical equilibrium, and estimate internal body loadings. In such models, the physiological properties of the muscles are based on the extensively studied Hill muscle model (3) which represents the muscle's force generating capacities as

Address for correspondence: Laurent Vigouroux, Ph.D., Aix-Marseille University, Institute of Movement Sciences, CNRS UMR 7287, 13288 Marseille, France; E-mail: Laurent.vigouroux@univ-amu.fr.
Submitted for publication December 2017.
Accepted for publication June 2018.
Supplemental digital content is available for this article. Direct URL citations appear in the printed text and are provided in the HTML and PDF versions of this article on the journal's Web site (www.acsm-msse.org).

0195-9131/18/5011-2311/0
MEDICINE & SCIENCE IN SPORTS & EXERCISE®

DOI: 10.1249/MSS.0000000000001690

APPLIED SCIENCES

a function of its specific characteristics (physiological cross-sectional area, optimal and slack length) and states (activation, muscle length [Lm], and muscle velocity). These characteristics are usually incorporated into musculoskeletal models to define the boundaries of muscle forces and define the optimization criterion function for solving the muscle redundancy problem (4). Among the different muscle characteristics, those concerning the force–length relationship are particularly important for modeling the hand. Grasping tasks imply large ranges of motion, this means that the hand muscles required in finger and/or wrist flexion operate over a wide range of fiber lengths, directly affecting their force-generating capacities (5,6). The force–length relationship is usually modeled with second-order exponential curves (7) that represent the decreased muscle force generating capacities for Lm distant from the optimal Lm.

Although force–length and force–velocity relationships have been studied and included in lower-limb models for many years, the upper-limb models often neglected these important aspects of the muscle contraction physiology (for review, see Buchanan et al. [8]). The currently most developed musculoskeletal models of the hand use muscle characteristics measured on cadaver specimens (9) or adjusted using optimization procedures (10). These approaches lead to inconsistencies in the modeled muscle force generating capacities as compared with the recorded performance of healthy individuals (11,12). Such discrepancies could be explained by the inherent limits of *in vitro* studies which, for example, depend on the dissection laboratory temperature (13) and on the specific characteristics of the specimens which can be nonrepresentative of *in vivo* behavior. Concerning the optimization-based methods used to adjust muscle properties, although the representation of each person's capacities is improved overall in the model, the values of each adjusted parameter could be underestimated or overestimated as a result of compensatory effects.

As an alternative to cadaver studies and indirect optimization assessment, ultrasound scanners represent an interesting way of evaluating muscle characteristics *in vivo*. Recent improvements in ultrasound scanners have enabled the development of methods for characterizing the contractile properties of the lower limb (14), such as the force–length relationship (15,16), the force–velocity relationship (17), or tendon stiffness (18). However, to our knowledge, only one study has used ultrasound methods to characterize the muscle properties of one muscle in the hand, that is, *first dorsal interosseous* (19). This lack of knowledge is mainly explained by both the high number of muscles located in the hand and their small size. Hence, localizing any hand muscle using an ultrasound probe is laborious (20). As a result, most of the studies using ultrasound were conducted on lower-limb muscles, which are more easily identifiable. Nevertheless, because no information is available, the influence of Lm on muscle force generating capacities remains poorly known.

Hence, the first aim of this study was to develop a novel method to investigate the force–length–activation relationships of hand muscles. As a first step, the flexor carpi radialis (FCR) (i.e., flexor of the wrist) and the flexor digitorum superficialis (FDS) (i.e., flexor of the fingers/wrist) were investigated as they are required for many hand movements and object manipulation. The second aim was then to compare the force–length–activation characteristics of these two muscles. A protocol was developed to simultaneously measure the change in Lm using *in vivo* ultrasound imaging, the moment exerted at the wrist and metacarpophalangeal (MCP) joints as well as the EMG activity of forearm muscles. By combining these measurements with the estimations of a musculoskeletal model, the muscle force–length–activation of the two muscles of the hand were determined for each participant (individual model) and for the entire population (average model). The obtained models were tested during additional contractions by comparing their estimations, only based on EMG and Lm, to those based on net moment measurements and those of other EMG models commonly used in the literature. Three hypotheses were formulated: (i) considering the differences in architectural properties and biomechanical functions of the two muscles (21,22), their force–length–activation relationships would differ, in terms of both curvature, that is, width of the plateau, and peak location, that is, angle where maximal force is reached; (ii) the interindividual variations of the estimated force–length–activation relationships would be small enough so that an average model can be used without introducing large errors; (iii) neglecting the force–length relationship will introduce larger errors on estimated muscle force at extreme angulations, since optimal length is usually closer to the mid-position of the joints.

MATERIALS AND METHODS

Participants. Eleven healthy males (25.5 ± 2.1 yr, 177.5 ± 5.2 cm, 73.2 ± 5.1 kg; hand length, 20.1 ± 0.7 cm) volunteered to participate in the study. Participants had no history of pathologies or injuries of the right arm. The participants were fully informed about the nature and aim of the study before giving their written informed consent. The study was conducted in accordance with the Declaration of Helsinki and was approved by the local ethics committee. The present study was divided into two sessions: the first was conducted on the wrist flexor muscles, FCR, and the second on the finger flexor muscles, FDS. Before the experiment, a reference length for the FCR muscle-tendon unit was measured from the medial epicondyle to the base of the second metacarpal, defined as the intersection between the line extending from the longitudinal axis of the index finger and the border of the thenar eminence. The FDS reference length was measured from the medial epicondyle to the middle of the index finger middle phalanx, as the index finger compartment of FDS muscle was targeted during ultrasound measurements.

The following methodology is organized in three different sections. The first section, "Protocol," describes the experimental design setup to evaluate the force capacities of the participants and to measure muscle behavior during isometric contraction. The second section, "Derivation of the force–length–activation

relationships from experimental data" describes the data processing required to model the relationship between muscle force, activation level and Lm. This section also presents how the force–tendon deformation relationship was computed to provide additional data for the purposes of literature comparison and to implement further modeling studies. Finally, in the third section, "Evaluation of the muscle force estimated by the experimentally derived relationships," we present the methodology required to validate the use of our three-dimensional (3D) relationship and compare the results with the data available in the literature.

Protocol. During the first session, corresponding to the FCR muscle, a custom-made hand ergometer (Bio2M, Compiègne, France) was used to perform isometric wrist flexion. The participants were standing with the right forearm to the horizontal and the joint elbow at 120° (180° corresponding to full extension). The axis of rotation of the wrist was aligned with the measurement axis of the ergometer. The subjects generated wrist joint torques by exerting forces on an aluminum plate positioned on the palm of their hand. The width of the aluminum plate was 2 cm so that the fingers and the thumb were not in contact with the ergometer or any other surface and were free to move. This configuration limits the contribution of hand extrinsic muscles in the wrist joint torque exertion (11). After a standardized warm-up, two maximal voluntary contractions (MVC) were performed with the wrist at 0° of flexion and abduction (i.e., neutral angle, positive/negative corresponding to flexion/extension). The participants then performed two progressive isometric ramps from 0% to 100% of their maximal force capacity (6 s) at five different wrist angles. These wrist angles were made possible by rotating the aluminum plate around the ergometer axis at 60°, 40°, 20°, 0°, and −30° (see Figure, Supplemental Digital Content 1, which presents the different joints positions, http://links.lww.com/MSS/B318). The order of conditions was randomized and a 2-min resting period was observed between each trial. Finally, the participants performed two "FREE" conditions at 0° and 40° of wrist angle, which consisted of 10 s of isometric contraction ranging from 10% to 90% of MVC with no abrupt changes of torque.

For the second session, corresponding to the FDS muscle, the protocol was identical to that of FCR except for the following points: the MCP axis of rotation was aligned with the ergometer measurement axis. The fingers were entirely in contact (from the base of the proximal phalanx to the tip of fingers) with a larger aluminum plate. The tested angles were a combination of wrist and MCP joint flexions to test a broad range of Lm (−30°/0°, 0°/0°, 0°/20°, 0°/40°, 20°/40° for the wrist/MCP angles, respectively, see Figure, Supplemental Digital Content 1, which presents the different joints positions, http://links.lww.com/MSS/B318).

The torque (τ) was digitized using a 12-bit analog-to-digital converter (MX-Giganet, Vicon Motion Systems Ltd, Oxford, UK) sampled at 2000 Hz. During all trials, ultrasound, EMG, and kinematic data were collected simultaneously. An ultrasound scanner (Echo Blaster 128, TELEMED, Lithuania) was used to observe the myotendinous junction during isometric contractions with a sampling frequency of 60 Hz. Depending on the session, the probe (10 MHz, 39 mm) was placed over the myotendinous junction of either the FCR or the index finger FDS (FDSi). The placement of the probe was checked by functional movements before each trial. The probe was manually oriented and firmly maintained on the skin by the experimenter during each trial. The EMG signals from FCR, FDS, *extensor carpi radialis longus* and *extensor digitorum communis* were collected using a wireless mini sensor system (Delsys Trigno, Natick, MA). These muscles were chosen for EMG recordings as they represent the main wrist and MCP flexors/extensors. The placement of the electrodes was determined using anatomical descriptions, palpations and functional movements, as well as display of the signals during functional movements (23). The EMG data were sampled at 2000 Hz. A five-camera motion analysis system (Vicon Motion Systems Ltd, Oxford, UK) recorded the coordinates in three dimensions of reflective markers placed on (i) the ergometer (three markers) to measure the joint angle, (ii) the ultrasound probe (three markers) to track the probe position, and (iii) the forearm (lateral humeral epicondyle and radial styloid) to track the position of the radius. The sampling frequency was set to 100 Hz.

Derivation of the force–length–activation relationships from experimental data. The entire data processing relied on custom Matlab scripts (The Mathworks, Natick, MA). τ was low-pass filtered at 5 Hz using a second-order Butterworth zero-phase filter. EMG data were band-pass filtered at 10 to 400 Hz, rectified, low-pass filtered at 3 Hz using a fourth-order Butterworth zero-phase filter and normalized using maximum EMG signal values recorded during MVC (EMG_{max}) to calculate the muscle activation level (AL) during the tasks. Kinematic data were low-pass filtered at 5 Hz using a fourth-order Butterworth zero-phase filter. τ, EMG, kinematic, and ultrasound data were resampled to obtain 30 and 60 samples for ramp conditions and free conditions, respectively.

The instantaneous muscle–tendon unit length (Lmtu) was calculated from the MCP (Θ_{mcp}) and wrist (Θ_w) joint angles using anthropometric models (24,25). From the B-mode images, the displacement of the myotendinous junction was tracked manually (Fig. 1C). The 3D coordinates of the myotendinous junction were calculated using three reflective markers placed on the ultrasound probe and the position of the myotendinous junction on the B-mode image. The Lm was estimated from the distance between the myotendinous junction and the placement of the reflective marker on the lateral humeral epicondyle, that is, muscle origin. The Lm change (ΔLm, equation 1) was computed as the difference between the actual Lm and the Lm at rest (i.e., Lm at the start of the isometric ramp, Lm_0).

$$\Delta Lm = Lm - Lm_0 \quad [1]$$

Three steps, described further in the sections below, were required to model the force–length–activation relationship. The overall modeling process is illustrated in Figure 1. First, the force generated by the muscle under consideration (i.e., FCR or FDS) was estimated using a hand musculoskeletal

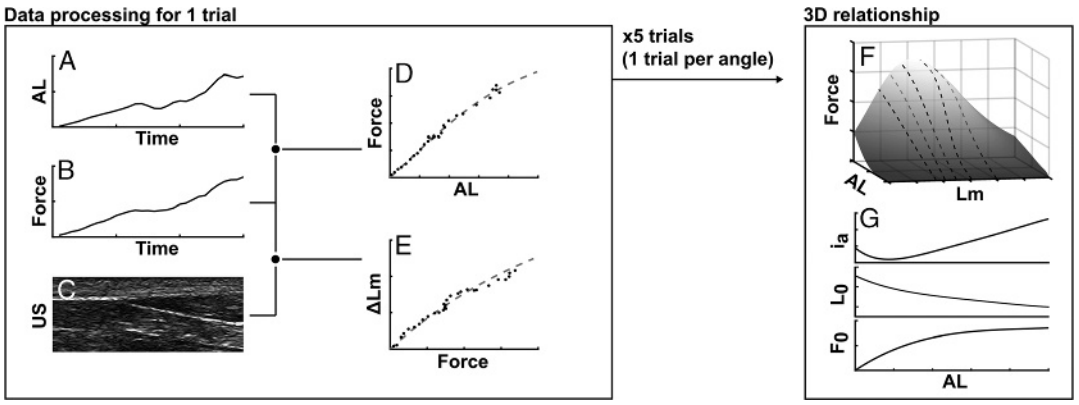

FIGURE 1—Individual example of force–length–activation relationship modeling. Collected data (A, C) and estimated force (B) were used to model force-activation (D) and Lm–force (E) relationships for all trials. Muscle force–length relationship was modeled from 5% to 100% of EMG_{max} (F). Maximal force (F_0), optimal length (L_0) and architecture index (a_i) were calculated (G) at each level of activation.

model involving all hand muscles (Fig. 1B). Second, the force–activation relationship and the force–length relationship were modeled for each trial (Figs. 1D and E). Finally, these two relationships were used to reconstruct a 3D relationship (force–activation–length relationship; Fig. 1F).

Step 1: estimation of muscle forces using hand musculoskeletal model. Estimation of muscle forces, including FCR and FDS muscle force, was done using a musculoskeletal model adapted from one previously developed in the laboratory (11,12,23) presented in supplementary data (see text, Supplemental Digital Content 2, which presents the estimation of muscle force, http://links.lww.com/MSS/B319). Briefly, for each trial of a participant, the model solved the muscle redundancy problem using an optimization procedure to estimate all the muscle forces required to balance the net moments measured on the ergometer (12). Generic data were used to represent the anatomy, that is, bone length, tendon moment arms and muscle physiological cross-sectional area, and scaled to each participant using hand dimensions (21,24).

Step 2: modeling of force–activation and length–force relationships. For each trial, a sigmoid equation was used to model a normalized relationship between force and AL (Fig. 1D) where the curve was constrained to pass through zero at the origin and increase to reach 1. Then, a normalized relationship between Lm change and force (Fig. 1E) was modeled using an inverse exponential equation with the same constraints as presented above:

$$\hat{f}_1(\mathrm{AL}) = a_1\left[\frac{1}{1+\exp(-a_2(\mathrm{AL}-a_3))} - 0.5\right] + a_4 \quad [2]$$

$$\hat{f}_2(F) = b_1\,[1 - \exp(-b_2 F)], \quad [3]$$

where a_1, a_2, a_3, a_4, and b_1, b_2 are unknown constants which have been determined using two successive optimization processes. The a values were determined in the first optimization process as follows:

Find a_1, a_2, a_3 and a_4 that minimize

$$\sum_1^{n=30}\left(f - \hat{f}_1(\mathrm{AL}, a_1, a_2, a_3, a_4)\right)^2 \quad [4]$$

subject to inequality constraints: $0 \le a_1 \le 1$; $0 \le a_2 \le 1$; $1 \le a_3 \le 10$; $0.1 \le a_4 \le 10$; and subject to equality constraint: $f(0) = 0$ and $f(1) = 1$.

Then, the second optimization process consisted in:

Find b_1 and b_2 that minimize

$$\sum_1^{n=30}\left(f - \hat{f}_2(F, b_1, b_2)\right)^2 \quad [5]$$

where n corresponds to the number of samples analyzed during the ramp.

Subject to inequality constraints: $1 \le b_1 \le 10$; $1 \le b_2 \le 10$ and subject to equality constraints: $f(0) = 0$

For each participant, the best fits of both trials were chosen at each tested angle using the method of least squares. All boundaries in the proposed methodological design were carefully fixed to obtain physiological results.

Step 3: 3D relationship reconstruction. Based on the relationships determined in step 2, the force–length relationship was modeled every 5% up to 100% of AL using force–AL and ΔLm–force relationships at each angle tested and the theoretical equation proposed by Otten (7) (equation 6; Fig. 1F).

$$f(\varepsilon) = \exp\left[-\left(\frac{(\varepsilon+1)^{\beta}-1}{\omega}\right)^{\rho}\right]F_0 \quad [6]$$

where F_0 and ε correspond to the maximal value of force and muscular deformation (equation 7), respectively.

$$\varepsilon = (\mathrm{Lm} - L_0)/L_0 \quad [7]$$

where optimal length (L_0) corresponds to the Lm when the force is maximal. The values of parameters ρ, β, and ω were given by Kaufman (26):

$$\rho = 2$$

$$\beta = 0.96343\,(1 - 1/a_i)$$

$$\omega = 0.35327\,(1 - a_i)$$

where a_i corresponds to the architecture index which influences the shape of the relationship. F_0, L_0, and a_i were

determined every 5% from 5% to 100% of AL by solving the following optimization problem (equation 8):

Find L_0, F_0, and a_i that minimize

$$\sum_1^{n=5}\left(f-\hat{f}(L_0,F_0,a_i)\right)^2 \quad [8]$$

where n corresponds to the five conditions of angles tested (see Figure, Supplemental Digital Content 1, which presents angles positions for wrist and fingers conditions, http://links.lww.com/MSS/B318).

Subject to inequality constraints: min (Lm) × 0.95 ≤ L_0 ≤ max (Lm) × 1.05; max (F) × 0.8 ≤ F_0 ≤ max (F) × 1.2; 0.01 ≤ a_i ≤ 0.7

L_0 values were normalized by the Lm at rest in neutral position (i.e., 0° for Θ_w and Θ_{mcp}). Individual optimal length, maximal force, and architectural index were used to calculate an individual 3D relationship for each participant. These parameters were then averaged between all participants according to the AL to obtain an average optimal length, maximal force and architectural index to then obtain a representative averaged 3D relationship. The following part of the methodological design presents the evaluation process of the obtained 3D relationships.

Derivation of the tendon force–deformation relationship. For literature comparison purposes and for a more detailed modeling, the tendon force–deformation relationship was also derived from the experimental data (see Document, Supplemental Digital Content 3, Modeling of force–tendon deformation relationship, http://links.lww.com/MSS/B320; see Figure, Supplemental Digital Content 4, Individual example of force–tendon deformation relationship modeling, http://links.lww.com/MSS/B321). Briefly, the actual tendon deformation was measured using ultrasound and was used to model a normalized relationship with muscle force determined during the isometric ramp performed in the neutral position.

Evaluation of the muscle force estimated by the experimentally derived relationships. To evaluate the obtained 3D relationships, we developed a dedicated EMG-to-muscle force model (EMG-driven model). The muscle force produced during the tested FREE conditions was estimated using the obtained force–length relationship, using only AL and ΔLm values, and compared with those obtained with the hand musculoskeletal model, based on τ values. This EMG-driven model estimates the muscle force using the relationships determined previously and the data measured during the FREE conditions. This evaluation procedure is illustrated in Figure 2 and detailed below.

For each FREE trial, τ, Θ_{mcp}, Θ_w, and EMG data were resampled to obtain 60 samples. Anthropometric and kinematic data were used to calculate the instantaneous Lmtu used as input to the function estimating the Lm at rest (Lm_0, Fig. 2A). EMG data were filtered, rectified, filtered and normalized to calculate AL. ΔLm was estimated using AL and the force–AL relationship and then the ΔLm–force relationship (Fig. 2B and C). Activation level was also used to determine the three parameters of the force–length relationship (i.e., a_i, L_0 and F_0). By combining Lm at rest and an Lm change, we predicted an instantaneous Lm. We thereby predicted the force produced using the Lm, i_a, F_0, and L_0 parameters and equation 6 (Fig. 2D). Three EMG-driven models were tested: (i) using the relationships determined for that participant (individual model), (ii) using the average relationship for all participants (average model), and (iii)

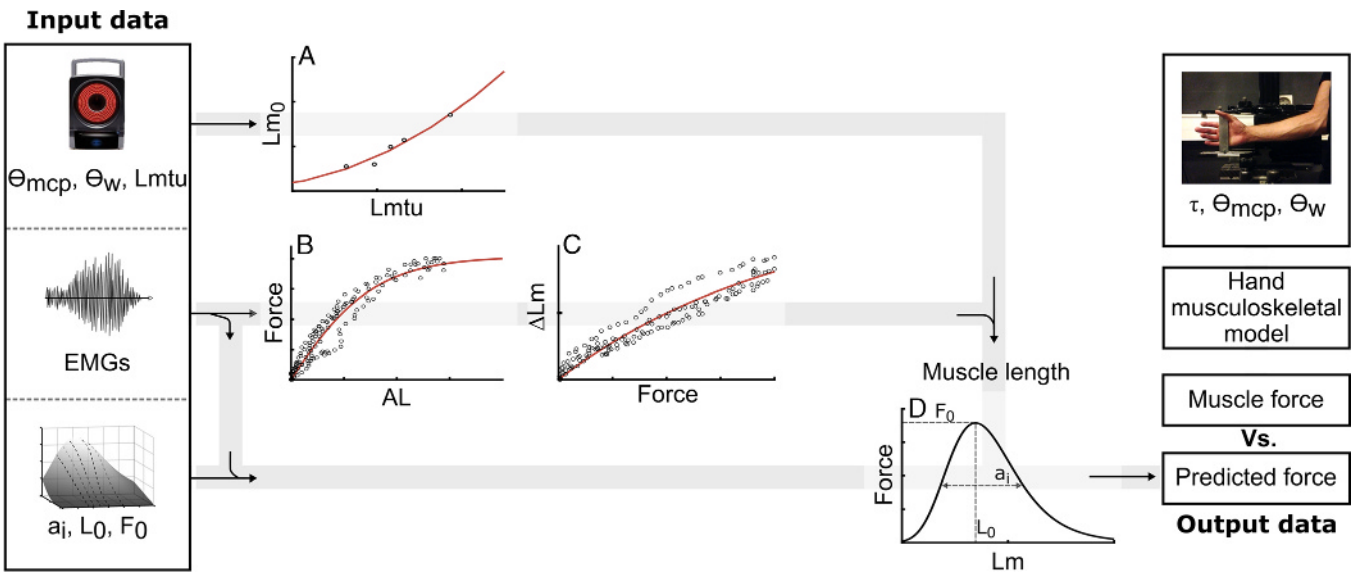

FIGURE 2—Schematic representation of the evaluation procedure. Anthropometric data, kinetic data, EMG data and 3D relationship parameters were the input data for the EMG driven model. The relationship between Lmtu and Lm_0 (A) was used to calculate the theoretical Lm at rest. Electromyographic data were used to estimate the ΔLm using the force–AL relationship (B) and the ΔLm–force relationship (C). The difference between Lm_{rest} and ΔLm corresponds to the predicted Lm. The AL was also used to determine a_i, L_0 and F_0 to plot the specific force–length relationship (D). This specific relationship and the predicted Lm enabled a muscle force to be predicted. Finally, the predicted force was compared with the muscle force calculated by torque and the hand musculoskeletal model.

TABLE 1. Mean ± SD of architectural and mechanical properties of musculoskeletal elements.

	Wrist	MCP
Mmax, N·m	19.1 ± 3.8	16.2 ± 3.6*
	FCR	**FDS**
F_{max}, N	460.6 ± 76.8	129.6 ± 32.8*
Lmtu, cm	34.4 ± 1.8	44.3 ± 1.9*
Lm, cm	19.4 ± 2.2	27.3 ± 2.0*
L_0, cm	18.6 ± 2.0	26.0 ± 2.1*
L_0 %Lm	95.4 ± 1.9	94.9 ± 1.7, ns
Lt, cm	13.1 ± 2.1	17.0 ± 0.7*
ΔLt_{max}, cm	1.0 ± 0.3	1.4 ± 0.4**
ΔLt_{max}, $\%Lt_0$	7.6 ± 2.3	8.1 ± 2.5, ns
k1	0.250 ± 0.14	0.272 ± 0.14
k2	1.606 ± 0.91	1.538 ± 0.62

Mmax, Lmtu, Lm, and Lt were measured with wrist and finger joints in neutral position. F_{max} and L_0 were estimated by individual 3D relationship. Maximal lengthening of tendon corresponds to the difference between the length at rest and the ΔLt_{max}. Significant difference between muscles: *$P < 0.001$, **$P < 0.05$.
Lt_{max}, length at maximal activation level; Mmax, maximal moment; Lt, tendon; ns, not significant.

without any adapted force–length relationship (predicted force = F_0; NoFL model). To evaluate the muscle forces determined by the EMG-driven model described above, the differences between predicted data from the three versions (i.e., individual model, average model, NoFL model) and the force calculated using the hand musculoskeletal model (see step 1) were computed. Root mean square error results (RMSE) for each tested version were normalized with respect to F_{max} (i.e., F_0 at 100% of AL).

Statistical analysis. Normality of the data was confirmed using the Shapiro–Wilk test. Statistica software was used to perform parametric statistical tests. The statistical differences between both muscles were tested using paired t-tests for architectural, muscle optimal length and stiffness properties. As a first step in validating our force estimation, one three-way ANOVA (muscle–angle–model) was performed to assess the statistical changes of RMSE results from the first two models (individual model vs average model) and determine the most appropriate. Then, 2 three-way ANOVA (FL × angle) were performed to assess the statistical effects of force–length relationship on RMSE results (Individual vs NoFL model) for each muscle. A Bonferroni *post hoc* analysis was conducted when appropriate. The level of significance was set to $P < 0.05$.

RESULTS

A summary of the measured muscle architectural and the estimated variables is shown in Table 1. The maximal forces produced at 100% of activation level (F_{max}) resulting from step 2, were, on average, 460.6 ± 76.8 N and 129.6 ± 32.8 N for FCR and FDSi, respectively (Table 1). The lengths of muscle–tendon unit, muscle and tendon for FDSi were significantly greater compared with FCR ($P < 0.001$). The corresponding optimal length normalized by Lm at rest in neutral position was not significantly different between muscles and was determined at 0.955 ± 0.019 and 0.947 ± 0.017 for FCR and FDS, respectively. The maximal tendon deformation was significantly higher for FDS compared to FCR ($P = 0.02$), but it was not different when the values were normalized with respect to each muscle's resting length ($P = 0.45$).

Modeling of force–length–activation relationship. Individual relationships between force, Lm and activation level obtained during step 3 of the process were well fitted by the force–length model (mean R^2 = 0.92 ± 0.07 and 0.87 ± 0.11 for FCR and FDSi, respectively). The average force–length–activation relationships for both muscles are shown in Figure 3.

The values of the parameters used to model the 3D relationships (i.e., a_i, L_0 and F_0) as a function of AL are shown in Figure 4 for both muscles. The values obtained for a_i were relatively independent of AL for FDS (average 0.22), while, for FCR, values increased with AL (0.19–0.35). Visually, the normalized optimal length of the FCR gradually decreased until maximal AL (0.99–0.95). For the FDS, the normalized optimal length decreased rapidly from 0% to 20% of AL (0.98–0.95) and then remained relatively constant for higher AL. The relationship between F_0 and activation level was not linear and was similar for both muscles.

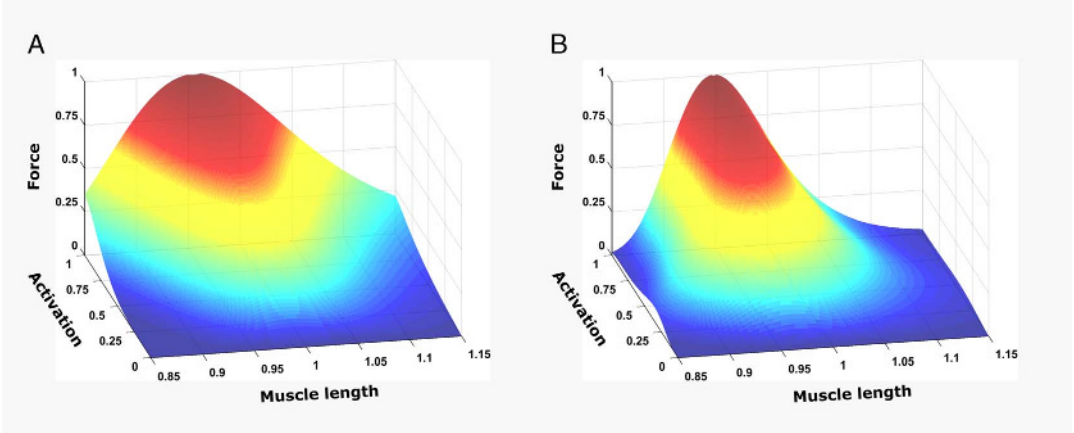

FIGURE 3—Average force–length–activation relationships of FCR (A) and FDS (B) muscles. Forces were normalized with respect to their maximal values. Muscle length was normalized using the Lm at rest with the joints in neutral position (i.e., 0°).

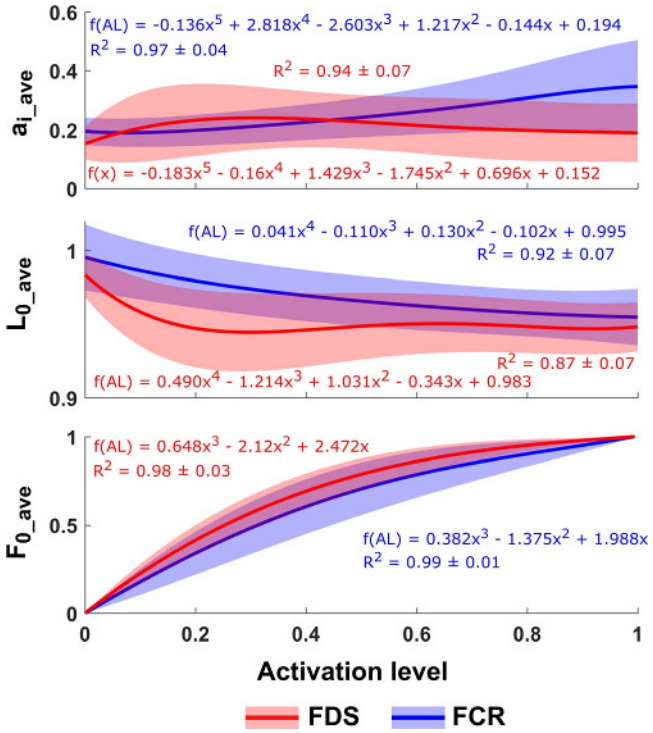

FIGURE 4—The average changes of architecture index (a_i), optimal length (L_0) and maximal force (F_0) according to the activation level for FDS (red line) and FCR muscles (blue line). The SD, coefficient of determination and polynomial functions used to fit each relationship are shown for both muscles.

Evaluation of the muscle force estimated by the experimentally derived relationships. An individual example of force estimation with the three EMG-driven models (individual, average, and NoFL models) is shown supplementary data (see Figure, Supplemental Digital Content 5, which presents force estimations, http://links.lww.com/MSS/B322). The results of the first three-way ANOVA (model–muscle–angle, Fig. 5A), which aimed to assess the statistical differences between individual and average models, were that the main "model" effect was significant ($P < 0.001$), whereas no main effects of "muscle" ($P = 0.11$) and "angle" ($P = 0.84$) were found. No interaction was found. As no significant effect of muscle and angle were found, the results shown in Figure 5A were obtained for both muscles and angles pooled together. The main effect of the model indicated that the force estimation errors obtained with the individual model were significantly lower than those obtained with the average model (6.9% ± 3.2% F_{max} and 8.5% ± 3.7% F_{max}, respectively).

Given that the Individual model presented the best RMSE results, the following analyses were carried out using the individual model. For FCR, the two-way ANOVA (FL–angle, Fig. 5B) showed that the main effects "FL" and "angle" were significant ($P < 0.001$). Interaction "FL–angle" was found ($P < 0.001$). The main effect of "FL" factor indicated that using the force–length relationship in the EMG-driven model for FCR resulted in better results. Moreover, the "angle" factor showed that lower RMSE values between EMG-driven and torque-based estimations were observed at 0° angle joint than 40°. The significant interaction between "FL" and "angle" factors showed that the RMSE results without consideration of force–length relationship at 40° (22.9% ± 8.1%) was significantly higher than at other conditions (7.1% ± 3.5%, 7.74% ± 4.1%, and 7.6% ± 3.3% for FL at 0°, NoFL at 0° and FL at 40°, respectively). For FDSi, the two-way ANOVA (FL–angle, Fig. 5C) showed that the main effect of "FL" was significant, whereas no main effect of "angle" was found ($P < 0.001$). No "FL–angle" interaction was found. The main effect of "FL" indicated that the RMSE values were lower with consideration of force–length relationship than without (6.6% ± 2.9% vs 8.3% ± 4.0%, respectively).

DISCUSSION

The aim of this study was to develop a new method to characterize of the force–length–activation relationships of the hand muscles. The originality of this method relies in the combination of musculoskeletal modeling together with

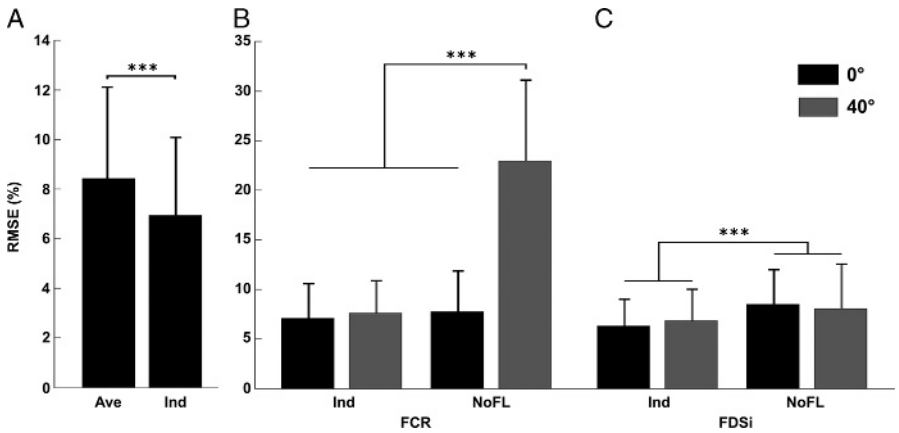

FIGURE 5—The RMSE (normalized with respect to F_{max}) and SD of force estimation for Individual (Ind) and Averaged (Ave) model are presented (A). Results of both muscles and angles were pooled. RMSE ± SD of force estimation calculated with (Ind) or without (NoFL) consideration of individual force–length relationship for both angles are shown. Results of FCR and FDSi are given separately (B, C). Significant difference between RMSE results: ***$P < 0.001$.

in vivo measurements of muscle/tendon deformations using ultrasound imaging as well as EMG activities to implement the 3D force–length–activation relationships of specific muscles. The 3D relationship varied in terms of both curvature and peak location between the two tested muscles, that is, FCR and FDS, indicating that the choice of dissociating the behavior of fingers and wrist flexor muscles was appropriate. Using the experimentally derived relationships, we developed an EMG-driven model to evaluate the accuracy of their muscle force predictions, especially compared to other models of the literature. The developed protocol as well as the collected data and the derived relationships contribute to the knowledge of hand function and muscle properties.

Muscle architecture of flexor carpi radialis and flexor digitorum superficialis. To implement the 3D force–length–activation relationships, the rest length and physiological properties of muscle and tendon were either measured ultrasound or estimated through the optimization processed based on other experimental data. The obtained data, presented in Table 1, are in themselves a significant contribution since, so far, the only available information about FCR and FDS muscle architecture has been obtained from cadaver studies (9,22,27,28). As mentioned in the Introduction, because of the anatomical complexity of the forearm musculature, ultrasound imaging had not been used to investigate hand muscles but its use in the present study demonstrated the feasibility and the interest of using such technique. The values of Lm estimated in this study (19.4 ± 2.2 and 27.3 ± 2.0 cm for FCR and FDS, respectively) were longer than values obtained on cadavers (16.3 ± 0.4 and 20.7 ± 1.1 cm for FCR and FDS, respectively; [9,22]). Such discrepancies might be explained by three factors. First, from a methodological point of view, we estimated the Lm as the distance from the myotendinous junction of the distal tendon to the muscle origin, that is, the lateral epicondyle. This value might thus overestimate the Lm as it also includes the length of the proximal tendon, which was not included in *in vitro* measurements. Unfortunately no data are available for the dimensions of the proximal tendon of FCR and FDS. Second, it is also possible that the specimens used in these previous studies were anthropometrically smaller, therefore resulting in shorter Lms; however, the anthropometry of these specimens was not communicated in the study of Lieber et al. (9). Finally, the length of an isolated muscle is dependent on its slack length, which might not correspond to its length in the neutral position, that is, the approach used in the present study. However, the relationship between muscle slack lengths and joint positions is not known for the hand, especially because most muscles are polyarticular, because their lengths depend on multiple degrees of freedom.

Overall, the FCR was stronger and shorter compared to FDS (Table 1). Optimal length, which corresponds to the Lm at maximal force, was also significantly different between both muscles. However, when optimal lengths were standardized (i.e., by length at rest in neutral position), there were no significant differences between both muscles ($P > 0.05$, 95.4% ± 1.9% and 94.9% ± 1.7%, for FCR and FDS, respectively). To provide a more detailed description of the muscles, it would have been interesting to have evaluated the muscle fascicle architecture (i.e., length, pennation angle, gear ratio, physiological cross-sectional area). The *in vivo* force–length relationship frequently includes such parameters because the muscle is often modeled at the fascicle level rather than at the belly level, as in this study. However, the probe frequency in this study was limited to 10 MHz therefore preventing a clear visualization of hand muscle fascicles and thin aponeurosis. Nevertheless, previous information available in the literature (9,22) indicated that pennation angle is low (<6°) and has thus probably little influence on the difference between hand muscle behavior and fascicle behavior.

Tendon properties of flexor carpi radialis and flexor digitorum superficialis. Some studies have worked on the automatic tracking of the *in vivo* displacements of hand tendons using ultrasound in a clinical context (29,30). Nevertheless, none of these studies have characterized the mechanical properties of hand tendons (e.g., deformation and stiffness). In this study, the displacement of myotendinous junction was complex, combining both changes in its orientation and position relative to bones such that the development an automated process would have been challenging. Thus, a manual tracking method was adopted. Here, the force–tendon deformation relationship and maximal deformation were measured using the isometric ramp in the neutral position for both muscles. The shape of the force–deformation relationship was approximately similar between both muscles, as could be observed from the comparable stiffness coefficients (k1 and k2, Table 1). The maximal deformation of the FCR tendon (1.0 ± 0.3 cm) was significantly less than the maximal deformation of the FDS tendon (1.4 ± 0.4 cm, $P < 0.05$). However, no significant differences appeared between both muscles when the values were standardized with respect to the tendon length at rest. These results showed that it is possible to estimate a maximal deformation of muscle and/or tendon using a simple measurement of muscle and tendon length at rest. Considering the maximal force of FCR and the similar tendon deformation, the FCR tendon stiffness could be higher as compared with the FDS tendon. Because no information is available about the cross-sectional area of these tendons, it is difficult to make clear conclusion as regards with the tendon stiffness of both muscles. Nevertheless, our results are consistent with muscle-tendon function. Indeed, FDS muscle is involved in a broad range of motion because it crosses two finger joints and the wrist, for a total angle excursion of approximately 330°; a compliant tendon is thus particularly appropriate for operating on the plateau of the force–length relation. On the contrary, the FCR muscle is only involved during wrist motions and thus over a more limited range of motion in daily activities, corresponding to the behavior of muscle with a stiffer tendon. Ward et al. (28) showed a maximal deformation of FDS tendon of 0.83% ± 0.04% on average from isolated tendons, which is considerably less than our results (8.1% ± 2.5%). This result could be explained by the different methods used

to estimate the maximal tendon deformation. Ward et al. predicted a muscle maximum tetanic tension using a theoretical equation proposed by Sack and Roy (31) and a muscle specific tension taken from the literature, that is, 22.5 $N \cdot cm^{-2}$ (32). However, recent studies showed that this value of specific tension underestimated the actual strength of young healthy participants (11,33). It is therefore possible that the previous studies that used this method to estimate the maximum tetanic tension also underestimated the tendon deformation levels. This important discrepancy between *in vitro* and *in vivo* experiments highlights the fact that care should be taken when considering the results of *in vitro* studies. This is particularly crucial for musculoskeletal models in which the maximal muscle force capacities are often estimated using data measured *in vitro*, thus creating inconsistencies between the modeled and the actual strength of the tested participants.

Force–length relationship. In addition to the results of architectural properties discussed above, the main contribution of this study is the experimentally derived 3D relationship of the muscle force–length–activation. Our methodological design presents satisfactory results for force–length modeling (Fig. 3, $R^2 = 0.92 \pm 0.07$ and 0.87 ± 0.11 for FCR and FDS, respectively).

Importantly, our results showed that the joint angles of the wrist and the fingers influenced the produced moment, which could be related to the muscle force–length relationship in accordance with the literature (34). These relationships have been already investigated *in vivo* at the muscle level for the lower limb (15,16) but only *in vitro* data were available for the hand (9). Typically, the force–length relationship is modeled using the equation proposed by Otten (7), see Equation 6, and an architectural index (a_i) that influences the shape of the relationship (ranging from 0 to 1). In the literature, this variable (a_i) is assumed to be equal to the muscle fascicle length divided by the entire Lm (9,26). An a_i close to 1 corresponds to a flat curve of force–length relationship (little effect of length on force), whereas conversely, 0 corresponds to a sharp curve (strong effect of length on force). The a_i of FCR estimated from the optimization procedure in this study (i.e., 0.35 ± 0.16 at F_{max}, Fig. 4) was in accordance with the literature (i.e., ranged between 0.31 and 0.39) (9,35,36). On the other hand, the value obtained here for FDS (0.19 ± 0.10 at F_{max}, Fig. 4) differed more significantly from those available in the studies mentioned above (from 0.34 to 0.76). This discrepancy is probably explained by the various approaches used to study the musculotendinous system of FDS. Some studies considered FDS as a single muscle (36), whereas others dissociated it into four compartments, each associated with one of the four long fingers (35). The lower a_i value obtained for FDS compared with FCR validates our hypothesis that these two muscles present different behavior as regard with their lengths and that it is necessary to investigate separately the mechanical behavior of finger and wrist muscles. Interestingly, the lower a_i value obtained for FDS indicate that its force-generating capacities are particularly influenced by its current length, for example, a shortening of 5% of the Lm induces a decrease in muscle force of 16% for FCR and 50% for FDS. Although no other studies provided *in vivo* data of this muscle behavior, studies focusing on the grasping of cylindrical objects found that participants exerted their maximal grip force for an optimal diameter, estimated at 17.9% of the hand length, and was decreasing beyond this value (37). This idea that the grip force capability is dependent on object size seems to be strongly related to force–length aspects since the cylinder diameter directly influences the finger and wrist joint posture, which in turn affects the current lengths of FDS and other hand muscles. Further study should thus investigate the link between optimal diameter of handle and optimal Lm. A hypothesis of the present model was that passive forces in the parallel element of Hill's elastic muscle model were negligible. The resistive torque measured at rest for the most extended positions in this study was close to zero, that is, $<0.5\ N \cdot m^{-1}$; therefore, meaning that passive forces indeed contributed little to the torques measured by the ergometer. It is however possible that such hypothesis would be inadequate to study positions out of the range tested here, for example, >30° of wrist extension. Although passive contributions were not quantified, the data and relationships obtained in this study provide crucial information about muscle contraction mechanics which could be useful for the design of hand tools or sports equipment, for example, to reduce fatigue or increase performance.

The EMG-driven model showed convincing results with low errors of force estimation for both muscles and both models (Fig. 5, $6.9\% \pm 3.2\%$ F_{max} and $8.5\% \pm 3.7\%$ F_{max} for individual and average models, respectively). Although significant, the differences between the errors of the individual and average models were low ($+1.5\% \pm 3.6\%$ F_{max}). Therefore, our second hypothesis that the values of the average model are generalizable to a healthy population is valid. A second analysis aimed at testing the force–length effect in our EMG-driven model (Fig. 5B and C) by comparing the individual model with the Individual model without force–length relationship (NoFL model). Globally, the inclusion of a force–length relationship in the EMG-driven model reduces the RMSE of muscle force estimates independently of the muscle or the angle tested ($P < 0.001$). Interestingly, the largest effect was observed for FCR at 40° of wrist angle (Fig. 5C), where the error of the NoFL model was more than three times greater than the one using the relationships derived in the present study. However, at 0°, the two models resulted in comparable levels of error. This result seems to indicate that between 0° and 40° of flexion, the FCR muscle is not operating on the plateau region and that its length significantly influences its force production capabilities. For this muscle, neglecting the force–length relationships could thus introduce large errors in the estimates of muscle forces, confirming that the length dependence of maximal force should be considered. However, for the FDS muscle, leaving out the force–length relationship did not seem to impact the estimation error.

Although this might indicate that force–length could be neglected, it is also plausible that the situation of two angles tested in FREE conditions for FDSi corresponds to a specific angle range where the muscle is operating on the constant part of force–length relationship (i.e., where the force capability is not affected by changes in muscle/fiber length). Because FDSi length depends on the angulations of three joints (wrist, MCP, and proximal interphalangeal joint), more joint configurations should be tested to identify where this dependency is the most critical in the entire range of motions.

Originality of the methodology. The main innovative contribution of this work is to provide an *in vivo* method to investigate muscle and tendon properties by combining ultrasound imaging and musculoskeletal modeling. This hybrid approach allows the derivation of the force–length relationship for a specific muscle in a complex musculoskeletal chain (as shown here with FDS and FCR muscles), based on the estimation of its contribution to a measured joint moment. The development of such method is particularly important for joints actuated by numerous muscles, like the wrist, which is also crossed by tendons acting at the finger and thumb joints. Although such hybrid approaches have already been developed for lower limbs (see Buchanan et al. (8) for a review), the investigation of hand muscles was challenging. First, the redundancy of muscles and joints involved in grasping tasks necessitated the development of a special ergometer and the development of associated musculoskeletal models to estimate the force produced by each muscle (11). Second, the considerable number of muscles in a confined space makes it difficult to identify the various structures of the musculoskeletal system on ultrasound images. These challenges were overcome and a new hybrid musculoskeletal model of the hand incorporating an individualized force–length relationship was developed. So far, hand musculoskeletal models have used *in vitro* information from cadaver studies to model muscle force capabilities. By providing information on the *in vivo* behavior of muscle contraction, this study provides new insight into the biomechanics at the wrist and finger joints.

The experimentally derived relationships were evaluated by using them in an EMG-driven model to estimate muscle forces solely based on Lm and activation levels and compare them with estimates from the musculoskeletal model, solely based on measured moment. Because of the muscle redundancy problem, a musculoskeletal model was used to estimate the contribution of FDSi and FCR muscles to the net moment measured on the ergometer. Although the used model has been validated through numerous studies concerning hand biomechanics (11,12,23) and provides quantification of internal loadings, such approach is associated with inherent limitations. Among these, generic data are used to represent the anatomy (muscle moment arms, muscle physiological cross-sectional areas, bone lengths) of each participant and hence their muscle capacities. However, direct measurements of muscle forces involve the use of invasive sensors and therefore remain ethically and technically challenging, especially when studying the hand which comprises numerous muscles, that is, more than forty. Therefore, despite its limitations, such biomechanical models represent the most suitable approach to answer our research question, that is, exploring the capacities of a specific muscle in a musculoskeletal system. Beyond these limitations, the errors obtained with the EMG-driven approach, using the derived relationships, resulted in small error, that is, below 10% of maximal force, therefore showing that the force of these two muscles can be accurately estimated using only Lm and activation levels as input, instead of a complex musculoskeletal model. Another novel aspect of this study was to model the force–length relationship depending on the muscle activation level (Fig. 3). Several relationships were established to take into account the fact that F_0, a_i and L_0 are dependent on the muscle's level of activation. Traditionally, a_i is considered as constant throughout the activation level; however, our results highlighted that this parameter tends to increase with activation, especially for FCR. This variation seems to corroborate the observation of pennation angle changes with the muscle contraction level (38). The effects of activation level on optimal length have already been described in the literature (39) and were attributed to a length dependence of calcium sensitivity (40). Nevertheless, in this study, we characterized the specific properties of FCR and FDS muscles compared with global estimates of the mechanical properties of whole muscles involved in grasping tasks as reported in earlier studies. This work thus offers new information to researchers and clinicians about physiological properties.

CONCLUSIONS

This study presents an accurate method for characterizing the mechanical properties and estimates the forces of hand muscles. Our results highlighted the importance of considering the force–length relationship in the EMG-driven model, especially in flexed positions, for the accurate estimation of muscle forces. This promising model is based on the EMG-driven and force–length relationship for agonist muscles but does not consider fiber contraction velocity; this means that it might not be suitable for applications other than isometric contractions. Thus, to improve this EMG-driven model and use it under dynamic conditions, further studies should investigate the effect of velocity on the force and muscle activity of antagonist muscles. Apart from its relevance to musculoskeletal modeling, the method and equations derived in this study could be used as a technique for evaluating individual characteristics of athletes or patients and to participate in a better understanding of the hand functions.

There were no external funding sources used in the preparation of this article. The authors declare that the results of the study are presented clearly, honestly, and without fabrication, falsification, or inappropriate data manipulation.

There is no conflict of interests concerning the preparation of this article. The publication of this article does not constitute endorsement by the American College of Sports Medicine.

REFERENCES

1. Dennerlein JT, Diao E, Mote CD Jr, Rempel DM. Tensions of the flexor digitorum superficialis are higher than a current model predicts. *J Biomech*. 1998;31(4):295–301.
2. Erdemir A, McLean S, Herzog W, van den Bogert AJ. Model-based estimation of muscle forces exerted during movements. *Clin Biomech (Bristol, Avon)*. 2007;22(2):131–54.
3. Zajac FE. Muscle and tendon: properties, models, scaling, and application to biomechanics and motor control. *Crit Rev Biomed Eng*. 1989;17:359–411.
4. Dumas R, Moissenet F, Lafon Y, Cheze L. Multi-objective optimisation for musculoskeletal modelling: application to a planar elbow model. *Proc Inst Mech Eng H*. 2014;228(10):1108–13.
5. Dempsey PG, Ayoub MM. The influence of gender, grasp type, pinch width and wrist position on sustained pinch strength. *Int J Ind Erg*. 1996;17:259–73.
6. Kong YK, Lowe BD. Optimal cylindrical handle diameter for grip force tasks. *Int J Ind Erg*. 2005;35:495–507.
7. Otten E. A myocybernetic model of the jaw system of the rat. *J Neurosci Methods*. 1987;21(2–4):287–302.
8. Buchanan TS, Lloyd DG, Manal K, Besier TF. Neuromusculoskeletal modeling: estimation of muscle forces and joint moments and movements from measurements of neural command. *J Appl Biomech*. 2004;20(4):367–95.
9. Lieber RL, Fazeli BM, Botte MJ. Architecture of selected wrist flexor and extensor muscles. *J Hand Surg [Am]*. 1990;15(2):244–50.
10. Colacino FM, Rustighi E, Mace BR. Subject-specific musculoskeletal parameters of wrist flexors and extensors estimated by an EMG-driven musculoskeletal model. *Med Eng Phys*. 2012;34(5):531–40.
11. Goislard de Monsabert B, Rao G, Gay A, Berton E, Vigouroux L. A scaling method to individualise muscle force capacities in musculoskeletal models of the hand and wrist using isometric strength measurements. *Med Biol Eng Comput*. 2017;55(12):2227–44.
12. Goislard de Monsabert B, Rossi J, Berton E, Vigouroux L. Quantification of hand and forearm muscle forces during a maximal power grip task. *Med Sci Sports Exerc*. 2012;44(10):1906–16.
13. Bottinelli R, Canepari M, Pellegrino MA, Reggiani C. Force–velocity properties of human skeletal muscle fibres: myosin heavy chain isoform and temperature dependence. *J Physiol*. 1996;495:573–86.
14. Narici M. Human skeletal muscle architecture studied in vivo by non-invasive imaging techniques: functional significance and applications. *J Electromyogr Kinesiol*. 1999;9(2):97–103.
15. Hoffman BW, Lichtwark GA, Carroll TJ, Cresswell AG. A comparison of two Hill-type skeletal muscle models on the construction of medial gastrocnemius length-tension curves in humans in vivo. *J Appl Physiol (1985)*. 2012;113(1):90–6.
16. Maganaris CN. Force–length characteristics of the in vivo human gastrocnemius muscle. *Clin Anat*. 2003;16(3):215–23.
17. Hauraix H, Nordez A, Guilhem G, Rabita G, Dorel S. In vivo maximal fascicle-shortening velocity during plantar flexion in humans. *J Appl Physiol (1985)*. 2015;119(11):1262–71.
18. Fouré A. New imaging methods for non-invasive assessment of mechanical, structural, and biochemical properties of human Achilles tendon: a mini review. *Front Physiol*. 2016;7:324.
19. Infantolino BW, Challis JH. Measuring subject specific muscle model parameters of the first dorsal interosseous in vivo. *Ann Biomed Eng*. 2014;42(6):1331–9.
20. Kawakami Y, Fukunaga T. New insights into in vivo human skeletal muscle function. *Exerc Sport Sci Rev*. 2006;34(1):16–21.
21. Chao EY, An KN, Cooney WP III, Linscheid RL. *Biomechanics of the Hand: A Basic Research Study*. Singapore, SG: World Scientific; 1989. pp. 53–72.
22. Lieber RL, Jacobson MD, Fazeli BM, Abrams RA, Botte MJ. Architecture of selected muscles of the arm and forearm: anatomy and implications for tendon transfer. *J Hand Surg [Am]*. 1992;17(5):787–98.
23. Vigouroux L, Goislard de Monsabert B, Hayot C, Androuet P, Berton É. Assessment of the risk and biomechanical consequences of lateral epicondylalgia by estimating wrist and finger muscle capacities in tennis players. *Sports Biomech*. 2017;16(4):434–51.
24. Buchholz B, Armstrong TJ, Goldstein SA. Anthropometric data for describing the kinematics of the human hand. *Ergonomics*. 1992;35(3):261–73.
25. Lemay MA, Crago PE. A dynamic model for simulating movements of the elbow, forearm, and wrist. *J Biomech*. 1996;29(10):1319–30.
26. Kaufman KR, An KN, Chao EY. Incorporation of muscle architecture into the muscle length–tension relationship. *J Biomech*. 1989;22(8–9):943–8.
27. Fridén J, Lovering RM, Lieber RL. Fiber length variability within the flexor carpi ulnaris and flexor carpi radialis muscles: implications for surgical tendon transfer. *J Hand Surg [Am]*. 2004;29(5):909–14.
28. Ward SR, Loren GJ, Lundberg S, Lieber RL. High stiffness of human digital flexor tendons is suited for precise finger positional control. *J Neurophysiol*. 2006;96(5):2815–8.
29. Korstanje JW, Schreuders TR, van der Sijde J, Hovius SE, Bosch JG, Selles RW. Ultrasonographic assessment of long finger tendon excursion in zone v during passive and active tendon gliding exercises. *J Hand Surg [Am]*. 2010;35(4):559–65.
30. Yoshii Y, Henderson J, Villarraga HR, Zhao C, An KN, Amadio PC. Ultrasound assessment of the motion patterns of human flexor digitorum superficialis and profundus tendons with speckle tracking. *J Orthop Res*. 2011;29(10):1465–9.
31. Sacks RD, Roy RR. Architecture of the hind limb muscles of cats: functional significance. *J Morphol*. 1982;173(2):185–95.
32. Powell PL, Roy RR, Kanim P, Bello MA, Edgerton VR. Predictability of skeletal muscle tension from architectural determinations in guinea pig hindlimbs. *J Appl Physiol Respir Environ Exerc Physiol*. 1984;57(6):1715–21.
33. Holzbaur KR, Murray WM, Delp SL. A model of the upper extremity for simulating musculoskeletal surgery and analyzing neuromuscular control. *Ann Biomed Eng*. 2005;33(6):829–40.
34. Delp SL, Grierson AE, Buchanan TS. Maximum isometric moments generated by the wrist muscles in flexion-extension and radial-ulnar deviation. *J Biomech*. 1996;29(10):1371–5.
35. An KN, Hui FC, Morrey BF, Linscheid RL, Chao EY. Muscles across the elbow joint: a biomechanical analysis. *J Biomech*. 1981;14(10):659–69.
36. Gonzalez RV, Buchanan TS, Delp SL. How muscle architecture and moment arms affect wrist flexion-extension moments. *J Biomech*. 1997;30(7):705–12.
37. Rossi J, Berton E, Grélot L, Barla C, Vigouroux L. Characterisation of forces exerted by the entire hand during the power grip: effect of the handle diameter. *Ergonomics*. 2012;55(6):682–92.
38. Narici MV, Binzoni T, Hiltbrand E, Fasel J, Terrier F, Cerretelli P. In vivo human gastrocnemius architecture with changing joint angle at rest and during graded isometric contraction. *J Physiol*. 1996;496(Pt 1):287–97.
39. Huijing PA. Important experimental factors for skeletal muscle modelling: non-linear changes of muscle length force characteristics as a function of degree of activity. *Eur J Morphol*. 1996;34(1):47–54.
40. Rassier DE, MacIntosh BR, Herzog W. Length dependence of active force production in skeletal muscle. *J Appl Physiol (1985)*. 1999;86(5):1445–57.